J. Astrophys. Astr. (2026) 47:14
https://doi.org/10.1007/s12036-026-10135-6

Global response of low and mid-latitude ionosphere to the severe geomagnetic storm of April 2023

VISWANATHAN LAKSHMI NARAYANAN

School of Interwoven Arts and Sciences, Krea University, 5655, Central Expressway, Sri City, Andhra Pradesh 517646, India.
E-mail: lakshmi.narayanan@krea.edu.in

MS received 31 January 2025; accepted 22 December 2025

Abstract. The response of topside ionosphere over low and midlatitudes to the severe geomagnetic storm of 23–24 April 2023 are studied using in-situ plasma measurements made by the Swarm satellite constellation at altitudes of 470 and 510 km. The local time coverage during the period was on dawn and dusk sectors. The geomagnetic storm is a two-step storm reaching a minimum SYM-H index magnitude of −233 nT. Observations reveal positive ionospheric storm with plasma density enhancements during sunlit periods of the main phase of the geomagnetic storm. This enhancement is significant over the Southern hemisphere. A clear increase in the equatorial electric field due to prompt penetration field is inferred through the increased separation of EIA crests and plasma density enhancements. This event showcased a longlasting prompt penetration electric field covering both the main phases. Interestingly, during the temporary recovery phase between the first and second main phases, the ionospheric observations are similar to those in the main phases with no indication of an overshielding electric field. During predawn hours of temporary recovery phase, a negative ionospheric storm is observed only over low latitudes. During the recovery phase, disturbed dynamo effects are also observed. However, for the first five hours in the early recovery phase, the effects were still similar to that of main phase. While the ring current recovery indicated by SYM-H indices took more than 36 hours, the disturbance dynamo effects were seen in the ionosphere only for about 11 hours, and the ionosphere was behaving similar to the quiet periods after 16 hours of start of the recovery phase. The observations are explained by means of undershielding prompt penetration electric fields during the main phases and development of disturbed dynamo effect well into the recovery phase.

Keywords. Geomagnetic storm—ionosphere—prompt penetration electric field—disturbed dynamo—overshielding electric field.

1. Introduction

The geomagnetic storms are major space weather events lasting for a few days and affecting the upper atmosphere and ionosphere globally (Gonzalez *et al.* 1994; Buonsanto 1999; Prölss 2008). Each geomagnetic storm is unique and hence case studies of such events continue to provide important new insights. At the same time, there is a general pattern in which the events affect the ionosphere which is reasonably understood. Almost all of the severe geomagnetic storms are caused by coronal mass ejections while the fast solar wind speeds from coronal holes can trigger prolonged moderate geomagnetic storms (Borovsky 2006). During the arrival of coronal mass ejection, a southward interplanetary magnetic field (IMF) B_Z component can lead to a dayside reconnection at the nose of the magnetosphere. This leads to the plasma convection in the magnetosphere, energization of the ring current and subsequent releases of energy within the system through the tail side reconnections triggering substorm processes (Lyon 2000; Borovsky 2021). The ionosphere receives energy input from the magnetosphere through the high latitudes. However, the ionosphere system has its own dynamo mechanism (Jin 2009) generating internal electric fields making the response a com-

This article is part of the Special Issue on "The evolution and space weather impact of coronal mass ejections".

Published online: 11 March 2026

plex one. Further, ionosphere is intricately connected to the neutral upper atmosphere through plasma-netural coupling processes thereby causing significant feedback mechanisms between the thermosphere and the ionosphere. Thus, the response of ionosphere to geomagnetic storms are complex and studies are being done to better understand how different upper atmospheric regions respond to geomagnetic activity (Laštovička 1996; Ranjan *et al.* 2023; Narayanan *et al.* 2024). Studying the mesosphere - thermosphere - ionosphere response to the space weather events become ever more important given our tech-savvy society's dependence on satellite technologies. At times, the upper atmosphere - ionosphere responds in unexpected manner leading to puzzling observations or unexpected technical difficulties (Narayanan *et al.* 2011; Baruah *et al.* 2024).

Despite the complexity, the low and midlatitude ionosphere is understood to respond in the following three ways. (i) The magnetospheric convection generates a dawn-dusk electric field that maps along the magnetic field lines through region 1 field aligned currents (FACs) into the high latitude ionosphere (Vasyliunas 1970; Wolf 1970; Vasyliunas 1972). At the same time, a partial ring current closes through region 2 FACs attempting to shield the dawn-dusk electric field by means of generating a dusk-dawn electric field (Wolf 1970; Vasyliunas 1972). Nevertheless, during intense magnetospheric convection this dusk-dawn field is weaker resulting in the mapping of high latitude dawn-dusk electric field into the low and midlatitudes instantaneously. This field is known as prompt-penetration (PP) electric field (EF) or sometimes as undershielding EF (Huang 2019; Kikuchi 2021). (ii) When there is sudden halt in the magnetospheric energy input due to a northward turning of IMF B_Z, (i.e. during a sudden drop in the polar cap potential), for few tens of minutes the dusk-dawn electric field caused by region 2 FACs will 'over shield' the PPEF (Peymirat *et al.* 2000). In such conditions, the low and midlatitudes are exposed to a dusk-dawn electric field that is typically westwards in the daytime and eastwards in the nighttime known as overshielding electric field (OSEF). It is very important to note that the above responses are ionospheric manifestations of an interlinked magnetospheric convection mechanism (Vasyliunas 1970; Wolf 1970; Vasyliunas 1972) (iii) The energy input from the geomagnetic storms in the high latitudes lead to significant thermospheric heating and an altered thermospheric circulation along with large scale traveling ionospheric disturbances. The thermospheric composition also changes during such conditions (Fuller-Rowell *et al.* 1994). In the quiet periods, maximum energy input occurs in the low latitudes from sunlight and this is altered during intense geomagnetic activity with maximum energy input in the high latitudes resulting in transport towards the equator from the polar region. The altered thermospheric wind circulation generates an ionospheric dynamo electric field that is nearly opposite to that of quiet time dynamo field. This is referred to as disturbed dynamo electric field (DDEF) (Blanc & Richmond 1980; Huang 2013). Note that the PPEF and OSEF are superposed on the existing ionospheric dynamo fields. The PPEF (OSEF) is similar (opposite) in direction to the ionospheric quiet time dynamo fields except in the terminator regions where there is large variability in the time of reversal of the fields. In the case of DDEF, the ionospheric dynamo itself gets altered. Nevertheless, there may be superposition of DD and OS fields in some cases, separation of their contributions is extremely difficult because of their similar directionalities.

The global response of low and mid latitude ionosphere (<50°geomagnetic latitude) to the geomagnetic storm of 23–24 April 2023 is the focus of the present paper. We are studying the global ionospheric response using in-situ electron density measurements made by Swarm satellite constellation and elucidate the predominant characteristics of the storm. In low and mid latitude ionosphere, an unmistakable feature existing for most part of the day is the equatorial ionization anomaly (EIA). Daytime eastward zonal ionospheric electric fields induce an upward plasma motion due to Lorentz force in the low latitude region where the geomagnetic field lines are nearly horizontal. This electric field action in combination with gravity and pressure gradient forces at altitudes above 200 km result in ambipolar diffusion of plasma along geomagnetic field lines resulting in a bimodal electron density distribution with electron density crests located on both sides of the dip equator at about 15–20 degrees geomagnetic/dip latitudes (Hanson & Moffett 1966; Balan & Bailey 1995; Batista *et al.* 2011). This process is also referred to as equatorial fountain in which the EIA forms in the morning hours and often observed until midnight. An evening strengtening of the feature may occur during strong prereversal enhancement (PRE) of electric fields around dusk. After sunset, the EIA usually decays slowly with equatorward approaching crests sometimes referred to as reverse fountain (King 1968; Narayanan *et al.* 2013). EIA plays an important role in inferring the direction of electric fields in the low and midlatitudes in this work. When the EIA is stronger and separated wider than quiet periods, it indicates a stronger eastward electric field, and vice versa. In addition to the strength of EIA, we

also use the measured electron densities to identify positive / negative ionospheric storms.

The effect of this storm has been studied over some specific geographical regions (Hajra *et al.* 2024; Mošna *et al.* 2024; Li & Jin 2024; Rao *et al.* 2025). To our knowledge, no study has investigated the global ionospheric behavior as done herein. In this work, we are studying the global ionospheric response using in-situ electron density measurements made by Swarm satellite constellation and elucidate the predominant characteristics of the storm. We do not consider longitudinal variabilities or impacts over particular geographical regions in this work. Given that we are making a case study, the intermittent measurements made by satellites renders meaningful investigation of longitudinal variations difficult and hence the focus is only on the overall ionospheric response in a global sense. In-situ electron density measurements also has limitations similar to any observational dataset from ground- or space-based platforms. Therefore, we carefully analyze and interpret the dataset in the context of existing knowledge on the effects of geomagentic storms on low and midlatitudes. The next section details datasets used, section 3 shows the results obtained along with the interpretations, and section 4 summarizes findings of this paper.

2. Datasets

The solar and geomagnetic indices that define the timeline of the geomagnetic storm are shown in Figure 1. The solar wind parameters plotted in the first three rows (Figure 1(a-c)) are obtained from NASA's Coordinated Data Analysis web (https://cdaweb.gsfc.nasa.gov/). Figure 1(d) shows the SuperMAG derived SME index (Gjerloev 2012) similar to that of AE index representing the strength of auroral electrojet. Figure 1(e) shows the ASY-H indices while Figure 1(f) includes both SYM-H index and another ring current index SMR derived from SuperMAG network. The SuperMAG indices are obtained from https://supermag.jhuapl.edu/indices/. The ASY-H and SYM-H indices are obtained from World Data Center for Geomagnetism, Kyoto (https://wdc.kugi.kyoto-u.ac.jp/index.html, Iyemori (1990)).

The ionospheric observations used to study the impact of the geomagnetic storm are obtained by Langmuir probe measurements made from the three satellite constellation Swarm operated by ESA (https://swarm-diss.eo.esa.int/). During the geomagnetic storm, Swarm A and C orbited at approximately 470 km altitude separated around 2 degrees longitude. Swarm B orbited at approximately 510 km altitude and was separated in local time by about 2.3 hours compared to the other two satellites, i.e. in a different longitude sector compared to Swarm A and C. The local time coverage of the satellites during this event falls in the dawn and dusk sectors, with A and C preceding in time. Typically, the satellite pair A and C pass before the solar terminator while Swarm B passes after the terminator. This is a unique configuration wherein the peak production heights of the ionosphere are in the dark before dawn during the measurements of Swarm A and C while Swarm B measures during fully sunlit ionosphere. Altitudes below 200 km are important for the ionospheric plasma production by photoionization and the plasma is redistributed through diffusion and other forces like electric fields and neutral winds to other heights (Rishbeth 1969). Therefore, identifying the sunrise at the plasma production altitudes below 200 km is important even when the actual height of the satellite may be sunlit. Otherwise, the local photoionization at the topside satellite altitudes will be negligible and plasma density variation is determined only through transport. Similarly, in the evening hours, Swarm A and C orbit in fully sunlit ionosphere before the sunset terminator in the early evening hours while Swarm B orbits after the sunset terminator in the lower ionosphere where photoionization is no longer happening.

The level 1b satellite data is used in this work, which are geotagged measurements of physical parameters with associated quality flags indicating the validity of the retrieved parameter. We have taken quality flags into consideration and only used good-quality data for the analysis. The electron density measurements are typically plotted for the required passes and duration with dip latitudes in the ordinate.

The timing of different storm phases are noted as will be described in the next section, and in order to see the effects of the geomagnetic storm in the ionosphere, we compare data during quiet periods three days before the storm (i.e. 20–21 April 2023) and three days after the storm (i.e. 26–27 April 2023) for the same durations of the identified storm phases. As can be seen from the magnetic indices, the periods are quiet making the comparisons sufficient enough for this storm.

3. Results and discussion

Figure 1(a-c) shows the solar wind drivers of the geomagnetic storm: interplanetary magnetic field (IMF) B_Z, solar wind pressure, earthward speed and interplanetary electric field (IEF) E_Y, respectively. IEF E_Y is

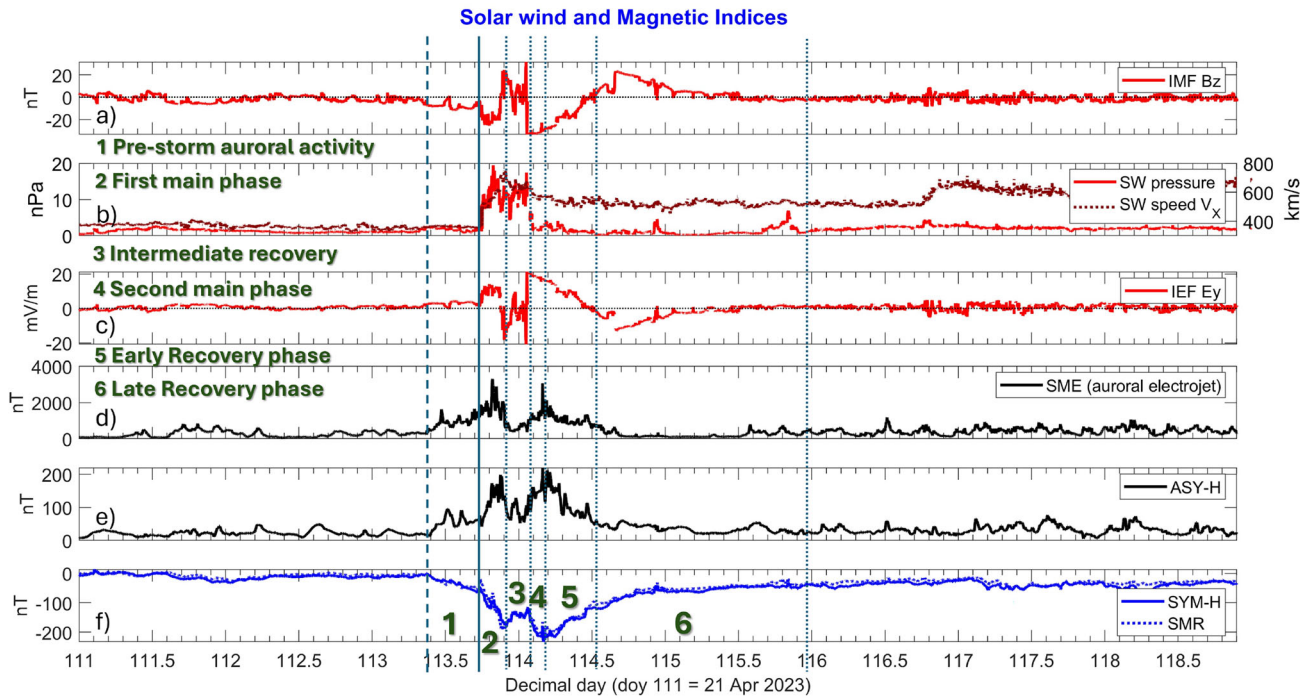

Figure 1. The solar wind and geomagnetic indices defining the different phases of the storm. **(a)** IMF B_Z, **(b)** solar wind dynamic pressure and earthward speed, **(c)** IEF E_Y, **(d)** SME index, **(e)** ASY-H index, **(f)** SYM-H and SMR indices.

calculated from earthward solar wind speed (V_X) and IMF B_Z as $E_Y = -V_X \times B_Z$. The magnetic indices are shown in Figure 1(d-f). The activity levels are separated into six phases as shown in Figure 1. The storm sudden commencement occurred at 17:36 UT on 23 April 2023. The first phase is the occurrence of an elevated auroral activity due to southward turning of IMF B_Z at ~9:46 UT on 23 April 2023, prior to the sudden commencement of the geomagnetic storm. A couple of isolated substorms were triggered by southward IMF B_Z before the arrival of CME shock as can be seen from SME and ASY-H indices in Figure 1(d-e). Because of these, SYM-H values were already below 0 nT during the sudden commencement. The second phase is the main phase onset at 17:41 UT following sudden commencement that occurred upon the impact of CME shock with a coincident reduction in IMF B_Z to −25 nT. This phase continued until 21:26 UT when the SYM-H index decreased to −179 UT. IMF B_Z suddenly turned northward following which there was a temporary recovery of the storm as can be seen from Figure 1(f) marking the third phase. SYM-H recovered to −125 nT at 24 April 01:36 UT. This storm had a second main phase triggered by sudden turning of IMF B_Z to −33 nT. From Figure 1(b), it may be seen that the solar wind dynamic pressure decreased with this IMF B_Z reversal indicating that it is the arrival of CME behind the shock that triggers the second main phase of the storm. The second main phase is the fourth phase of the storm. The peak of this severe storm occurred with SYM-H index dipping to −233 nT at 04:03 UT on 24 April 2023. The fifth and sixth phases of the event correspond to the long recovery phase of the storm.

The recovery phase started at 04:03 UT on 24 April and we consider the storm to be over when the SYM-H index continuously stayed around −40 nT or above. Note that for comparisons with quiet periods post the storm, we took data from the evening of 26 April and hence the SYM-H has recovered from the storm effects by then. Herein, the recovery phase of the storm is separated into fifth and sixth phases. They are respectively named as early recovery phase and late recovery phase. The early recovery phase is until 12:28 UT on 24 April 2023 when the IMF B_Z remained negative. As far as the IMF B_Z is negative, there will be energy input into the magnetosphere driving convection, and hence we separate the recovery phase based on the IMF B_Z. The end of the storm is considered in this study to be SYM-H attaining −40 nT and above in a consistent manner, which happens at 22:58 UT on 25 April 2023. Conventionally, weak geomagentic storm is said to be in progress when SYM-H is ≤ -30 nT. In this case, we take a slightly larger value as end of the storm because there was an enhancement in the solar wind pressure

during 15:58–21:46 UT on 25 April, which appears like a compression shock that coincided with weak negative IMF B_Z. This would have led to a delay in the recovery of the SYM-H index above −30 nT by initiating weak magnetospheric convection as indicated by SME and ASY-H indices. Further, SMR index already shows values ≥ −30 nT by 17:14 UT of 25 April with a slight reduction afterwards coinciding with the pressure pulse. Therefore, our selection of SYM-H ≥ -40 nT as the end of storm is a reasonable choice supported by SMR ≥ -30 nT and existence of a pressure pulse with weak negative IMF B_Z delaying the recovery of the storm under consideration.

3.1 *Main phases*

Figure 2 shows the dawn sector observations during main phases of the geomagnetic storm in comparison with quiet periods before and after the storm. For main phases, we combined both the first and second main phases during which period, the SYM-H index was decreasing and IMF B_Z was negative. The durations are 17:41 UT - 21:26 UT on 23 April and 01:36–04:03 UT on 24 April for the storm main phases. Same timings are compared on 21 and 22 April for quiet period before the storm onset, and on 26 and 27 April after the storm recovery. The first row (Figure 2(a-c)) shows measurements prior to storm onset, the second row (Figure 2(d-f)) shows observations during the storm main phase, and the bottom row (Figure 2(g-i)) displays observations during quiet periods past the storm. The first, second and third columns respectively show the observations from Swarm A, C and B.

By comparing rows 1 and 3 with row 2 of Figure 2, Swarm B shows a clear enhancement in the plasma density during main phases of the storm in the dawn sector around 7.8 LT. Note that Swarm B measures the ionosphere well after sunrise in the production region of 100–200 km (see previous section). Swarm A and C orbits at 5.4 LT, just around the time of ionospheric sunrise. Probably there was not enough plasma produced to clearly reveal a large difference in the densities at satellite altitudes of ∼470 km for Swarm A and C at ∼5.4 LT. Further, the direction of PPEF will be westwards in the nighttime. The observation of a Northern Hemispheric enhancement only in 165° E longitude sector may be a manifestation of longitudinal variability, which is not a focus of this paper. The increased plasma densities observed in Swarm B can be attributed to the lifting up of the ionosphere by means of prompt penetration electric field. This is because in the altitudes of Swarm B, in-situ production is negligible and hence such enhancements cannot be attributed to photoionization at satellite altitudes indicating that plasma transport in the presence of PPEF would have resulted in the increase.

Figure 3 shows observations during the dusk sector in the same format as in Figure 2. Here the Swarm B measurements are made at ∼19.8 LT while Swarm A and C are made at ∼17.5 LT. The major difference in the dusk sector observations between Swarm A and C and those of Swarm B is that the former are measured prior to the PRE in zonal electric field while the later after the PRE. Generally the evening reversal in the direction of ionospheric electric field happens after 20 LT in the equatorial region (Fejer & Scherliess 1997). Therefore, it is likely that the PRE is enhanced by the eastward directed PPEF during the geomagnetic storm. This inference is based on the observation of strong perturbations to the plasma densities all the way upto the equatorial ionization anomaly crests, and that the location of equatorial ionization anomaly crests themselves occur at around ∼20-25° dip latitudes as seen in Figure 3(f). Such strong perturbations will be caused by equatorial plasma bubbles (EPBs) (Spogli & Alfonsi 2023), which in turn are well known to be caused by stronger PREs around sunset periods. It may be noted that the EPBs also occurred during quiet periods before the storm as could be seen from Figure 3(c) shown for the night of 20 April. In most longitudes wherever the geomagnetic equator is parallel to the geographic equator, except in the South American and Eastern Pacific sectors, post sunset EPBs have a seasonal preference to occur during equinoxes (Maruyama & Matuura 1984; Tsunoda 1985; Kepkar *et al.* 2020) due to favorable alignment of magnetic field lines with the sunset terminator. Similarly, in the Brazilian sector, peak EPB season happens in December solstice when sunset terminator aligns closely with the strong westward declination values. However, in addition to the terminator alignment, other factors such as strong conductivity gradients, intense seed perturbations, electric fields, formation of steep vertical gradients, downward neutral winds can all affect formation of EPBs during post sunset hours on a given night (Narayanan *et al.* 2014; Carter *et al.* 2018; Currie *et al.* 2021), Therefore, observation of dusk sector post sunset EPBs on 20 April before the onset of geomagnetic activity is not a surprise. In this case, a careful comparison between Figure 3(c) and 3(f) clearly shows that the crest locations of equatorial ionization anomaly occurred poleward on the disturbed night of 23 April. This indicates the existence of prompt penetration electric field. Therefore,

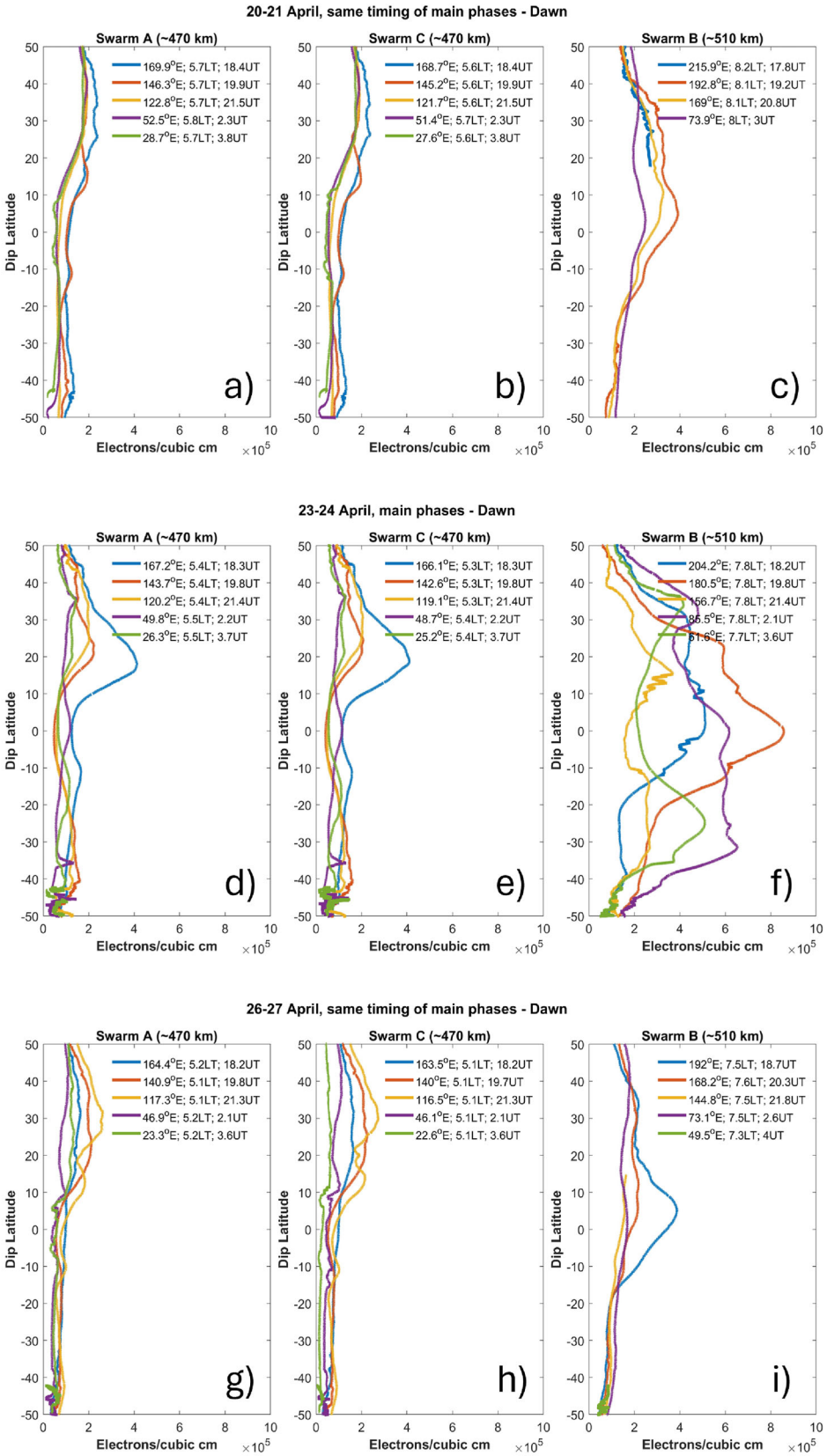

Figure 2. Dawn sector observations during the main phases. **(a-c)** quiet time observations before the storm from Swarm A, C and B respectively, for the same timings of the main phases on 20–21 April, **(d-f)** observations during the main phases on 23–24 April, **(g-i)** quiet time observations after the storm on 26–27 April.

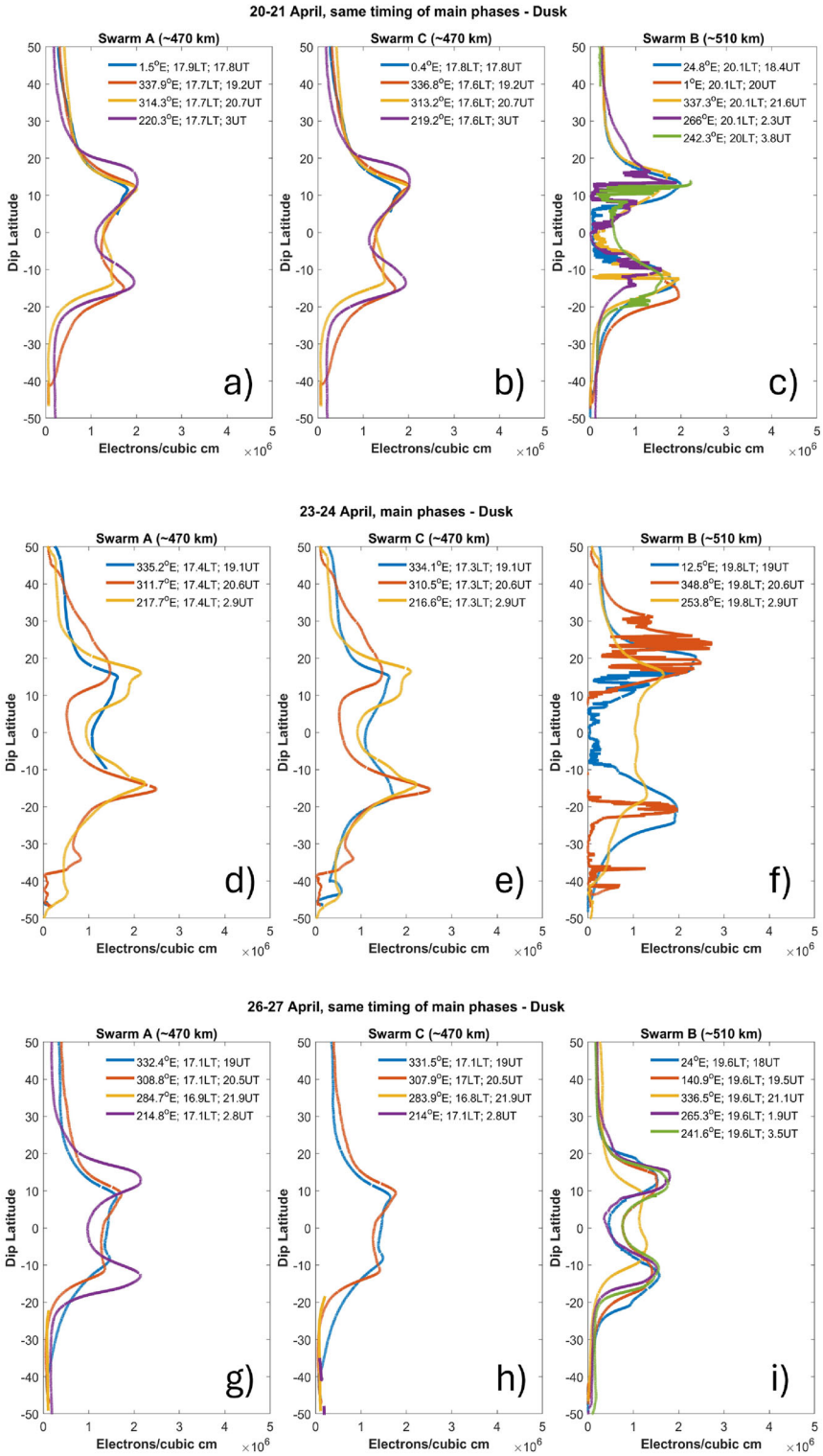

Figure 3. Dusk sector observations during the main phases in same format of Figure 2. **(a-c)** and **(g-i)** are quiet time observations before and after the storm, respectively. **(d-f)** observations during the main phases on 23–24 April.

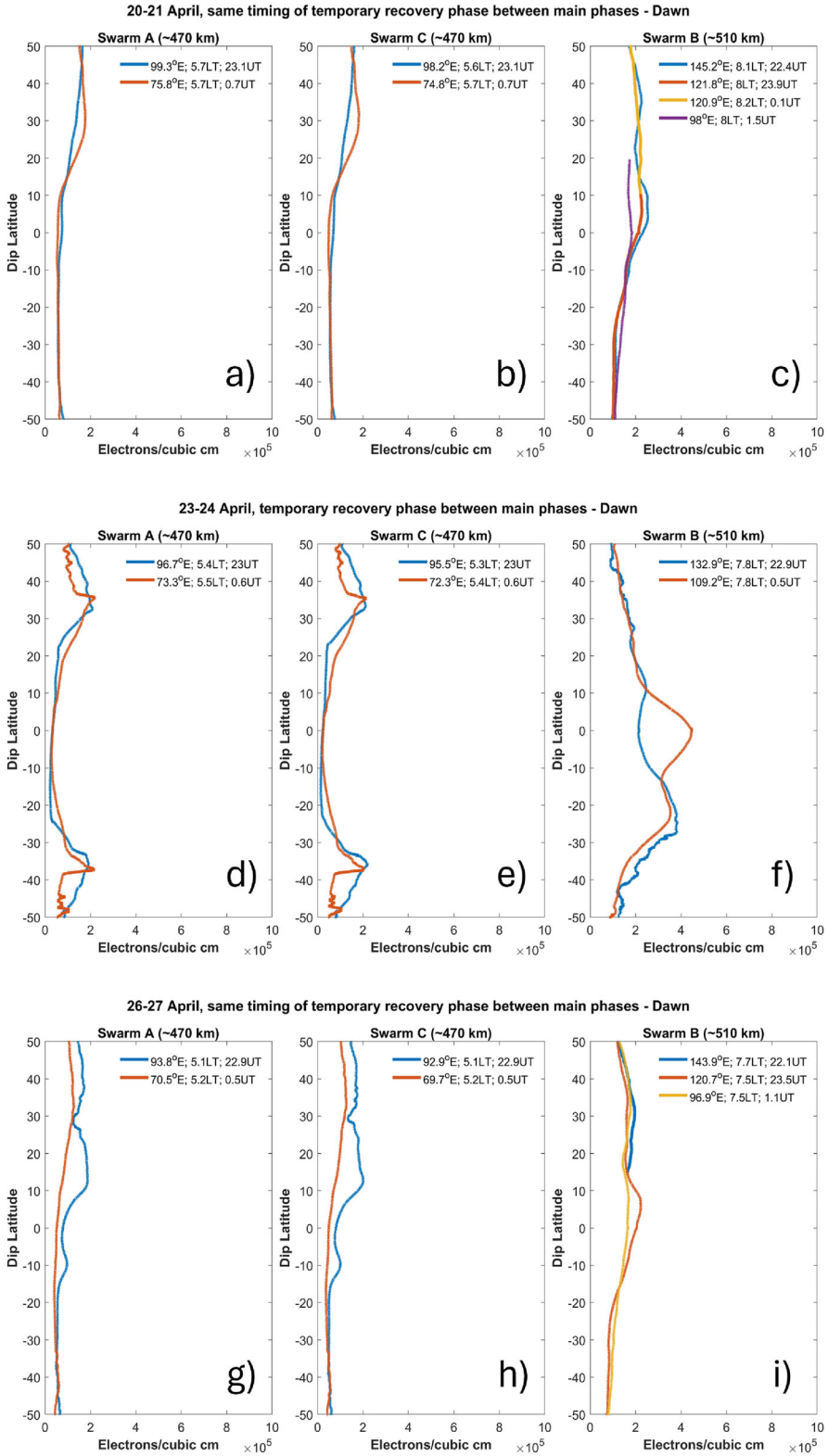

Figure 4. Dawn sector observations during the intermediate temporary recovery phase between the main phases in same format of Figure 2. **(a-c)** and **(g-i)** are quiet time observations before and after the storm, respectively. **(d-f)** observations during the main phases on 23–24 April.

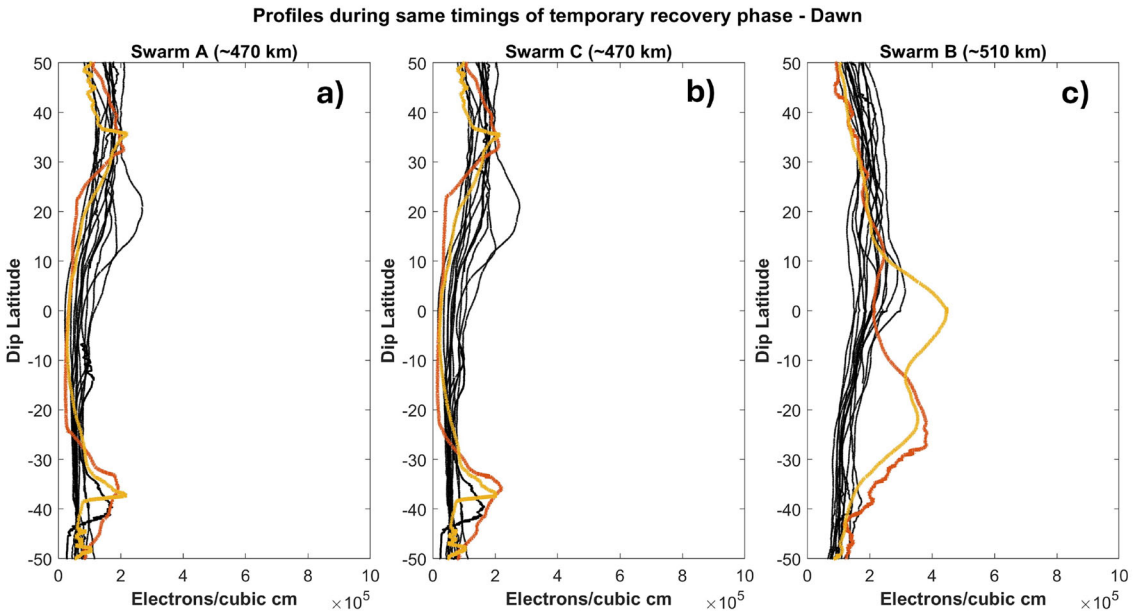

Figure 5. Dawn sector observations during the temporary recovery phase between the main phases. The thin black lines show all the profiles observed between 21:26 and 01:36 UT on the nights of 20–22 April and 26–28 April 2023, corresponding to quiet time profiles. The thick colored lines indicate the profiles observed during the temporary recovery phase on the night of 23 April, the same profiles shown in Figure 4**(d-f)**.

during both the dawn and dusk sectors, Swarm B indicates clear role of prompt penetration electric fields. The PPEF apparently contributed to the positive ionospheric storm during dawn sector, and stronger EIA along with generation of equatorial plasma bubbles in the night sector.

3.2 *Temporary recovery phase*

The most interesting phase is the temporary recovery phase between the first and second main phases. From Figure 1, it may be seen that this phase coincides with a sharp northward turning of IMF B_Z that continued for about 4 hours. Ideally, the magnetospheric convection would have abruptly interrupted allowing build-up of region 2 currents and development of OSEF having polarity opposite to that of the PPEF (Peymirat *et al.* 2000; Huang 2019; Kikuchi 2021). However, the results for this event shows otherwise as discussed below. Figure 4 shows the observations in the dawn sector during the intermediate temporary recovery phase between first and second main phases. Swarm A and C clearly shows a negative ionospheric storm below 20° dip latitudes, while Swarm B shows a positive ionospheric storm in comparison to the quiet periods. The penetration electric fields are expected to reverse around the solar terminators between Swarm A, C local times and Swarm B local time. Therefore, a westward field pushing existing plasma downwards into the recombination dominated region would have occurred for Swarm A and C just around the ionospheric sunrise. This effect is prominent in the topside only below 20° dip latitudes probably because the equatorward neutral winds from high latitude energy input would have hindered the downward movement of plasma when geomagnetic field lines become sufficiently tilted. Interestingly, a westward electric field in the pre-sunrise period is possible if it is a PPEF and not for a OSEF indicating that a PPEF was present in the temporary recovery phase as well. On the other hand, Swarm B measurements reveals enhanced plasma densities in the post-sunrise local times ensuring the presence of an eastward electric field. This is also possible only for a PPEF and not for an OSEF at ∼7.8 LT. The plasma density enhancements in Swarm B are more pronounced over the equatorial and Southern hemispheric regions.

It may be noted that the Swarm B measurements during quiet and distubed periods are separated by about 11-12° in longitudes. The validity of comparison may be questioned. As already mentioned, this work focuses only on ionospheric variability in a global sense during the different phases of the geomagnetic storm. Since, no particular longitudinal region is focused herein, the comparisons are valid and this can be further ascertained by Figure 5. Figure 5 shows all the profiles measured

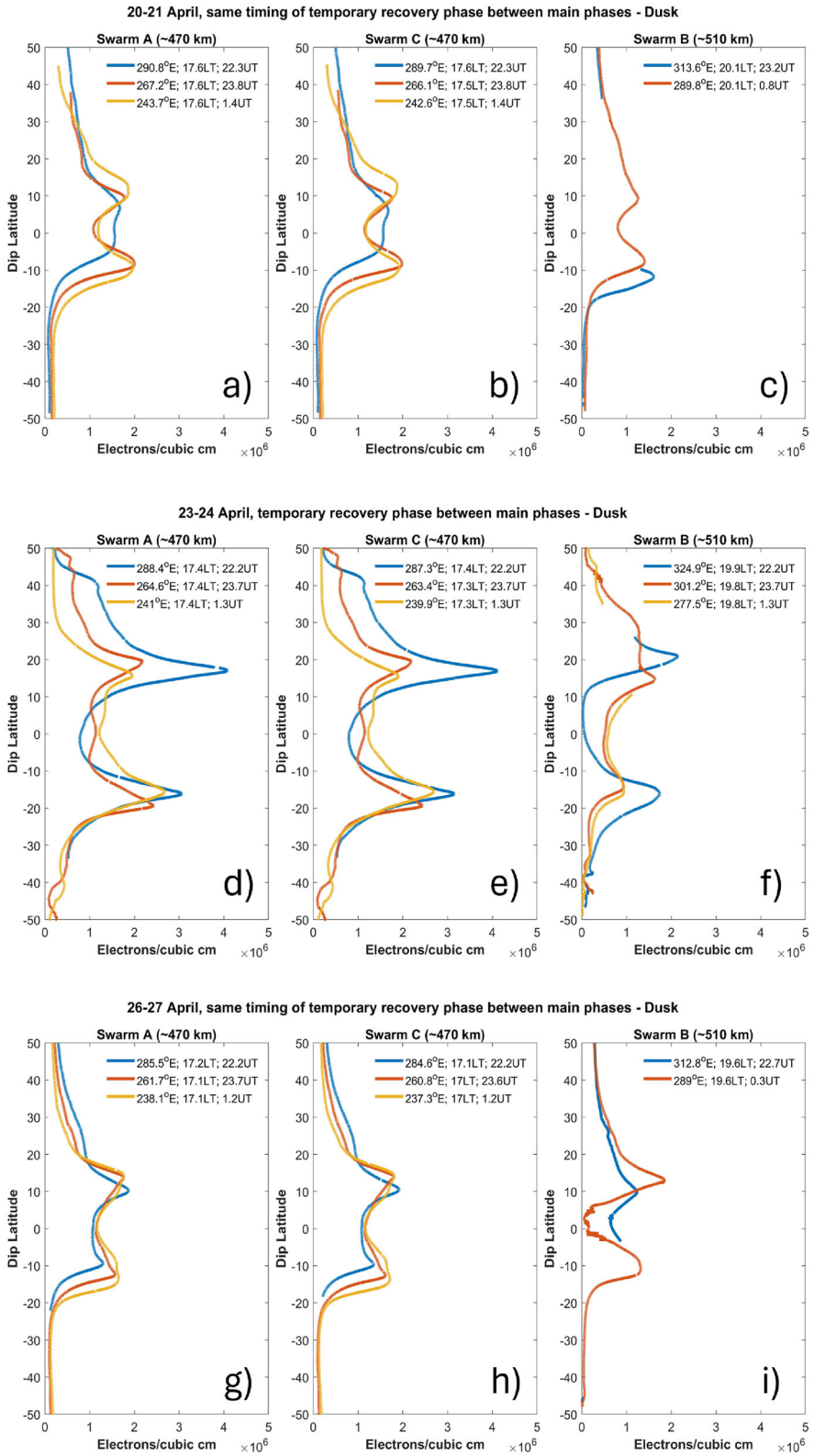

Figure 6. Dawn sector observations during the intermediate temporary recovery phase between the main phases in same format of Figure 2. **(a-c)** and **(g-i)** are quiet time observations before and after the storm, respectively. **(d-f)** observations during the main phases on 23-24 April.

during quiet periods between 21:26 - 01:36 UT on the nights of 20-22 April and 26-28 April in thin black lines. The disturbed period measurements in the temporary recovery phase during 21:26 - 01:36 UT on the night of 23 April are shown with thick colored lines. As one may see, clear enhancement is seen in Swarm B only during the disturbed period. This validates our comparison and such is the case for other phases of the event that are discussed in this work (though figures are not shown to avoid redundancy). From Figure 5, it may also be verified that the reduction in electron densities only in the low latitude region below 20° dip latitudes is observed through Swarm A and C. If there was an OSEF penetration during the intermediate recovery phase, we would have expected an opposite effect with Swarm A and C showing EPBs, or plasma density enhancements and Swarm B showing a negative ionospheric storm. This has not happened clearly displaying existence of PPEF similar to that of the main phases, contrary to the expected OSEF in the dawn sector.

Figure 6 displays the measurements from the dusk sector during temporary recovery phase. All the three satellites show well developed EIA crests with larger crest to through amplitudes and larger separation between the Northern and Southern crests in comparison to the quiet periods before (Figure 6(a-c)) and after (Figure 6(g-i)) the storm. The dusk side EIA development is larger than that during main phases in this duration of northward IMF B_Z driven intermediate temporary recovery phase. Again such an observation implies at the existence of strong eastward electric field amplifying the PRE, typical of PPEF undershielding fields. Another interesting observation is that despite such strong PRE, no EPBs formed. Anyhow, no signature of OSEF is identified in the topside ionospheric measurements during the 4 hours of temporary recovery phase. This might be due to the significant compression of day side magnetosphere by an enhanced solar wind plasma pressure (see Figure 1b) eventhough the IMF B_Z was northwards (Rout *et al.* 2016).

3.3 *Early Recovery phase*

Figure 7 shows the observations during early recovery phase. The first two columns show results from dawn sector and the next two from dusk sector. From Figures 2-5, one may notice that the satellites A and C show nearly the same information measured about 1.5 - 2.0° apart in longitude. Also because quiet time behavior of the ionosphere before and after the storm are similar, we show results only from satellites C and B from quiet period before the storm and during the early recovery phase of the storm. Hence, Figure 7(a and b) and Figure 7(c and d) respectively shows results from quiet and storm times for the dawn sector. Swarm C satellites reveal existence of EPBs close to the sunrise terminator at 5.4 LT. These early morning EPBs are strong in some longitudinal sectors, and it indicates the likely hood of their generation later in the night due to the an eastward electric field. Generally the EPBs either decay in these hours or will become fossilized and weak (Narayanan *et al.* 2016). It is well known that during the recovery phase of geomagnetic storms nocturnal DDEF will be eastwards and it can lead to formation of EPBs (Abdu 2012; Lyu *et al.* 2022). Almost all of the early morning EPB onset reported in the literature has occurred during geomagnetically disturbed conditions due to the DDEF. It may be noted that we are not referring to the post midnight EPBs generated during solar minimum periods (Otsuka 2018), but those intense EPBs observed in the early morning and post sunrise hours. Therefore, the intense early morning EPBs are most likely result of an eastward DDEF.

Another interesting observation supporting a disturbed storm time wind circulation is revealed by dawn sector observations of Swarm B data shown in Figure 7(b and d). Note that the latitudinal gradients during quiet time in Figure 7(b) and that during early recovery phase in Figure 7(d) are reversed. The gradient was decreasing from Northern to Southern hemispheres in quiet time (technically northward gradient), indicating probable presence of a North-South transequatorial meridional wind across the hemispheres. Such a wind will lift up the ionosphere resulting in a higher plasma density in the northern hemisphere and push the ionosphere to relatively lower altitudes along the field lines to cause larger recombination and lesser densities. Though the observation period falls in the spring equinox, late April is closer to the summer and hence such a wind can be expected. The observation of the reversal in the measured plasma density gradient can be taken as indication of the reversal of the wind pattern. This is expected since the thermospheric winds in their simplest mode can be explained as moving from low to high latitudes owing to larger solar illumination in the low latitudes. During disturbed conditions more energy input occurs at high latitudes and when the wind pattern becomes opposite to that of quiet time pattern, opposite nature of dynamo fields are generated that are known as DDEF. Therefore, the observation of a reversed latitudinal electron density gradient during the early recovery phase indicates the altered wind circulation.

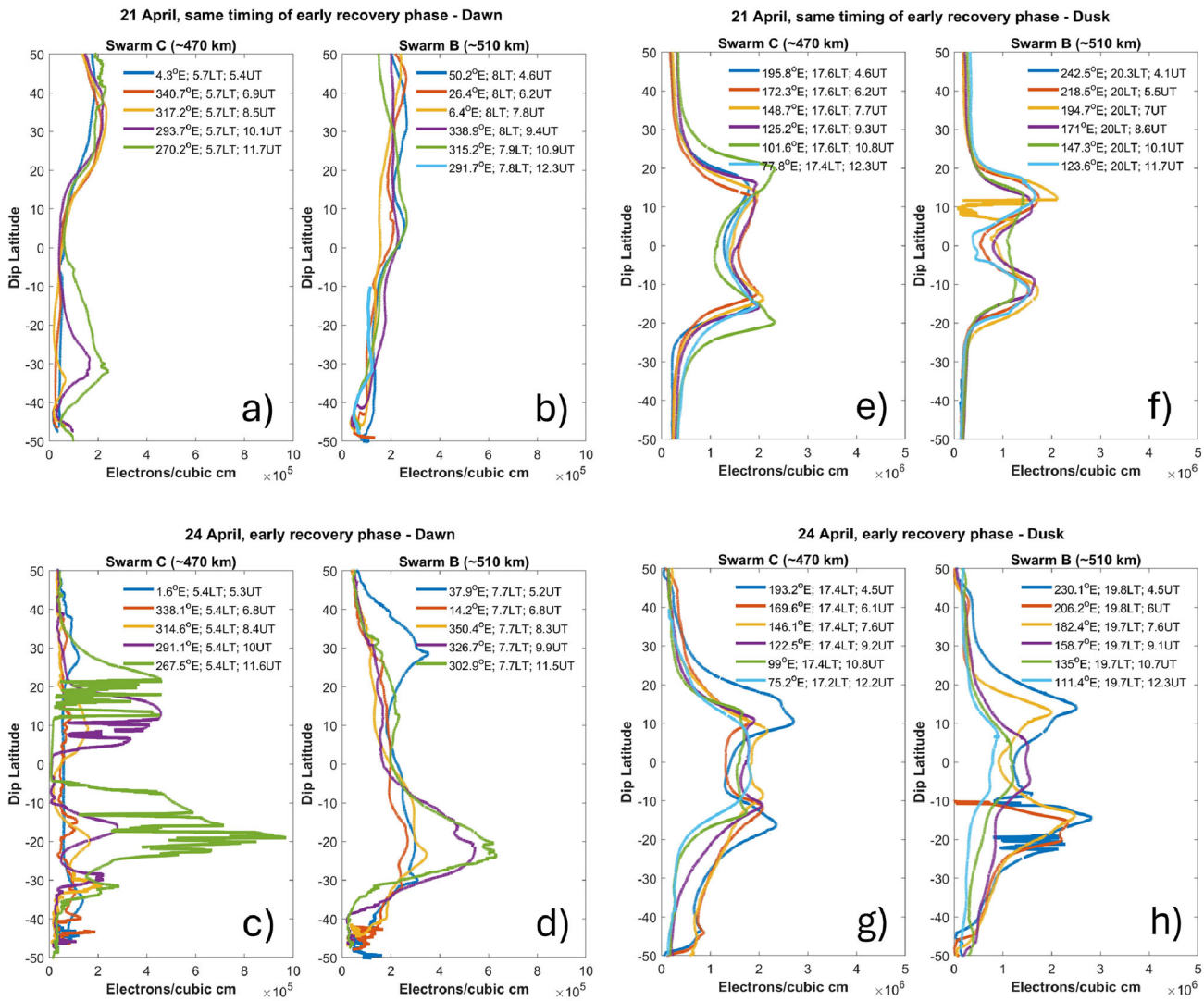

Figure 7. Observations during the early recovery phase. **(a-d)** Dawn sector with **(a-b)** showing Swarm C and B observations before the storm, and **(c-d)** showing Swarm C and B observations during the storm. **(e-h)** Dusk sector with **(e-f)** showing Swarm C and B observations before the storm and **(g-h)** showing observations during the storm.

The dusk sector results are shown in Figure 7(e-h). It may be seen that many longitudes show a reduction in the distance between the EIA crests during the early recovery phase while some longitudes show clear enhancement. While this appear to indicate some longitudinal variability, a careful analysis shows that the profiles before 9:00 UT have all shown an enhanced plamsa density and those after 9 UT shows an inhibition of EIA. This indicates that the DD electric field has set in between 8:00 - 9:00 UT. Figure 8 shows this clearly by separating the duration of early recovery phase further into two parts, before 9 UT and after. Note that Figure 8(e and f) shows an enhanced plasma density and well developed EIA crest while Figure 8(g and h) show inhibition of EIA development indicating opposite nature of electric fields. Interestingly, such an effect can also be seen in the dawn sector from Figure 8. The profiles after 9 UT in Swarm C contains intense EPBs, an after-effect of DDEF. With this we identify the approximate time of onset of the DDEF during this event. Though the energy input started from main phase onset, the altered thermospheric circulation generates DDEF only after 4 hours into the recovery phase.

3.4 *Late recovery phase*

Figures 9 and 10 shows the results during late recovery phase in the dawn and dusk sectors respectively. Note that late recovery phase is defined as the period from northward turning of IMF B_Z at 12:27 UT on 24 April

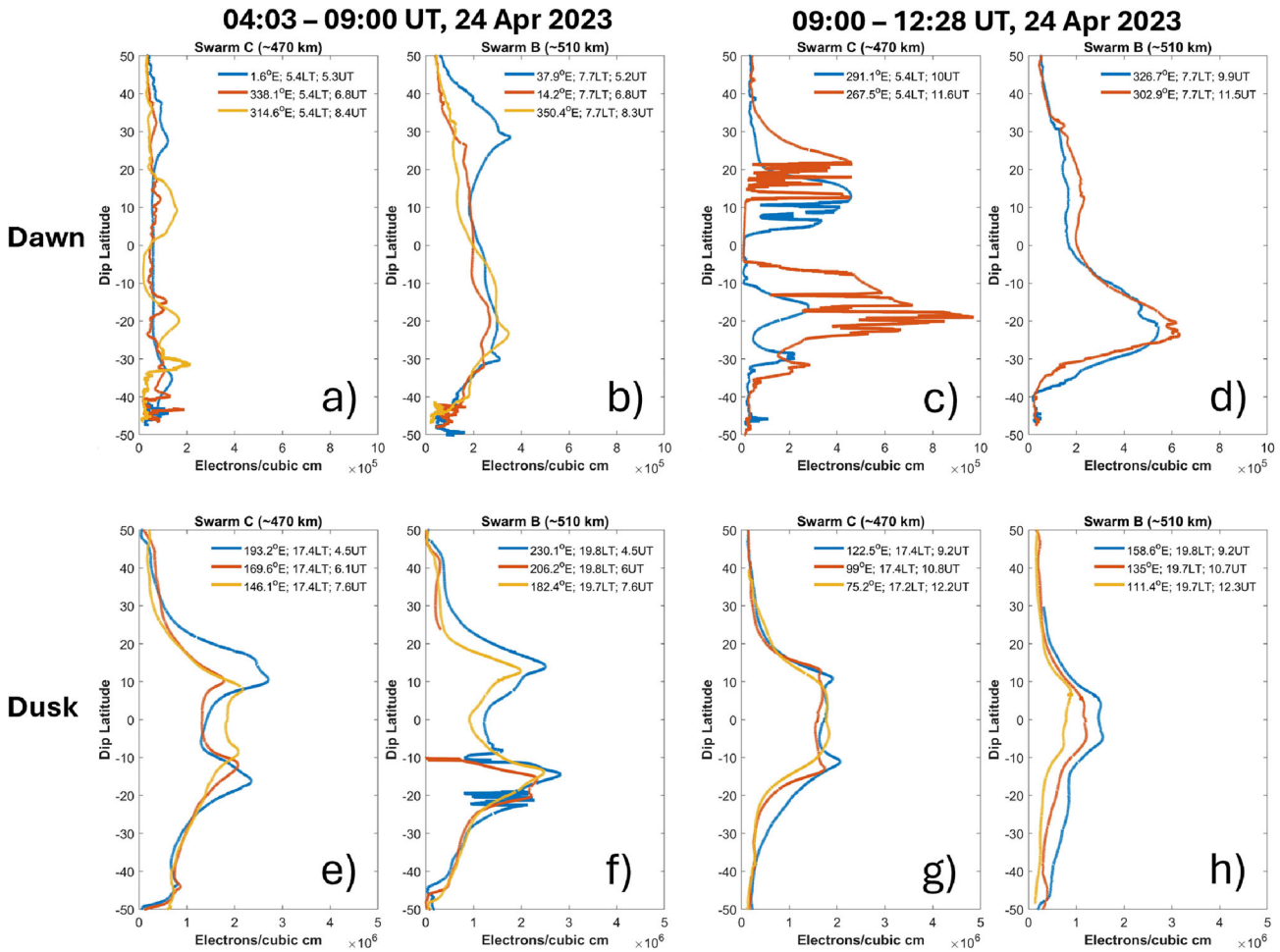

Figure 8. Observations during the early recovery phase of the storm on 24 April separated into two parts. **(a-b)** Swarm C and B data in the dawn sector between 04:03 - 09:00 UT, **(c-d)** Swarm C and B data in the dawn sector between 09:00 - 12:28 UT, **(e-f)** Swarm C and B data in the dusk sector between 04:03 - 09:00 UT, **(g-h)** Swarm C and B data in the dusk sector between 09:00 - 12:28 UT.

to the recovery of the storm with ring current index SYM-H reaching -40 nT and above at 22:58 UT on 25 April 2023. This phase lasted for 34.5 hours in total. To better visualize the large number of profiles sampled in this period, we have plotted them as three sets as given in Figure 9. Similar to Figure 7, Figures 9 and 10 also display only results from Swarm C and B for the same reasons mentioned earlier.

In the first period between 12:27 and 22:59 UT on 24 April, significant EPBs and enhanced plasma densities are noticed in all the three satellite measurements in Figure 9(c-d) in comparsion to the quiet periods shown in Figure 9(a-b) and 9(e-f). This appears to be a continuation of the observations during early recovery phase post 9:00 UT after the onset of DDEF. From a comparison of Figure 10(c-d) with those of Figure 10(a-b) and Figure 10(e-f), it may be seen that there was a suppression of EIA development due to the DDEF.

In the second and third periods of late recovery phase corresponding to 00:00 - 22:58 UT on 25 April shown in Figure 9(g-r) and Figure 10(g-r) for the dawn and dusk sectors, the behaviour of the ionosphere measured by Swarm satellites does not show profound differences during the storm time, as seen for the earlier phases for this event. The plasma density variations resemble normal day to day variabilities of the ionosphere. For example, Figure 9(n) shows that the ionospheric densities were relatively higher over some longitudes during quiet period on 22 April 2023, well ahead of the onset of the disturbances including the pre-storm auroral activity phase. Therefore, the implication is that the major storm effects in the ionosphere subsided well before the SYM-H index showed recovery of the ring current. To identify approximately when the DD effect has subsided, we further investigated the period between 12:27 - 23:59 UT on 24 April 2023. The results are

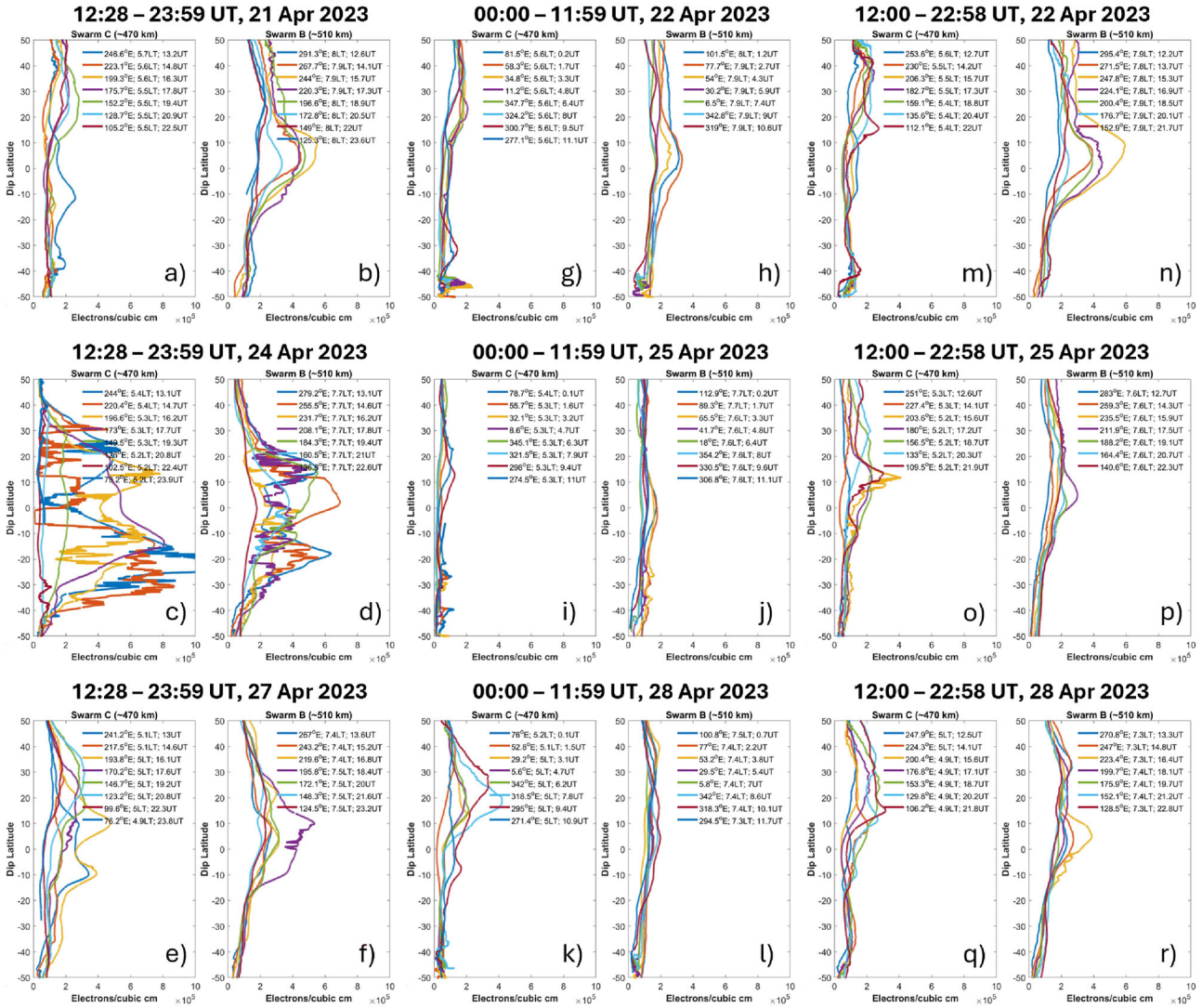

Figure 9. Swarm C and B observations are shown for the dawn sector in the late recovery phase. For better visualization, the duration is split into three parts of approximately 12 hours. The top and bottom rows show quiet time observations before and after the storm onset, respectively. The middle row shows storm time observations. **(a-f)** shows observations during 12:28 - 23:59 UT of 21, 24 and 27 April respectively corresponding to before, during and after the storm in the late recovery phase. **(g-l)** shows observations during 00:00 - 11:59 UT on 22, 25 and 28 April respectively. **(m-r)** shows observations during 12:00 - 22:58 UT on 22, 25 and 28 April respectively.

shown in Figure 11, which is similar to that of Figure 8 in its format. Note that the dawn sector results show a striking difference between profiles taken before 20:00 UT and after 20:00 UT on 24 April 2023. Profiles after 20:00 UT resemble that of quiet periods. In the dusk sector Swarm B observations clearly indicate a difference in that double humped EIA structure is clear in the profiles after 20:00 UT. Thus, based on these observations, we can conclude that the DD effect has declined by 20:00 UT on 24 April in the topside ionosphere. From Figures 8 and 11, DDEF is felt from 9:00 - 20:00 UT for about 11 hours during this storm recovery.

From the Figures, a careful reader may notice existence of strong longitudinal variabilities on some occassions. As already mentioned, we reiterate that we do not address longitudinal variability herein and provide a global picture. This is because of the nature of the intermittent satellite measurements used. To discuss the longitudinal variations effectively, we may need to combine ground and satellite measurements from different longitude sectors or we should analyze multiple storms. Nevertheless, interesting insights obtained from this work are described in the Summary section below.

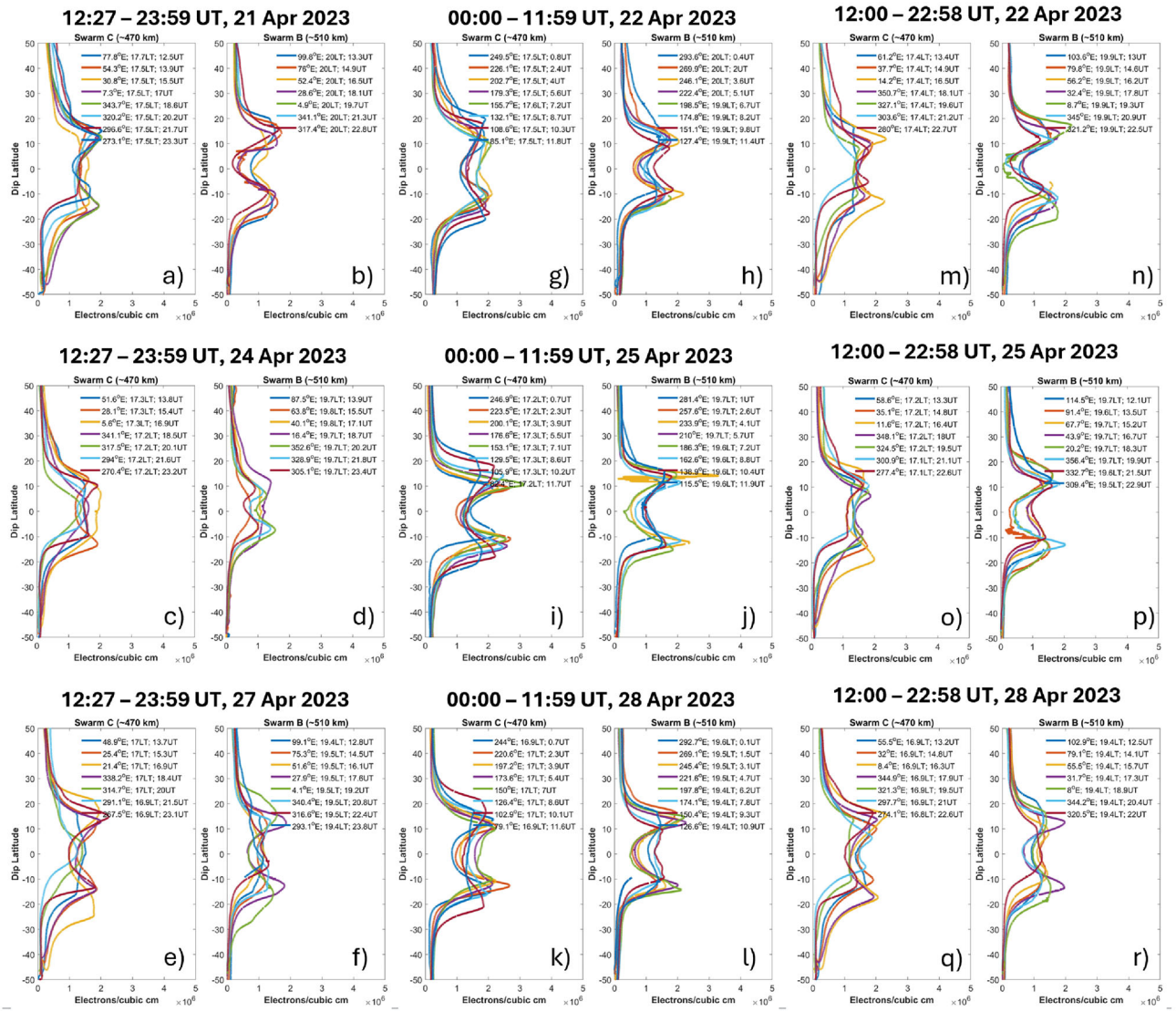

Figure 10. Swarm C and B observations are shown for the dusk sector in the late recovery phase. The Figure is of the same format of Figure 9.

4. Summary and conclusion

In this work, we discussed the global ionospheric response in low and midlatitudes upto ∼50° dip latitudes based on Swarm measurements in the topside ionosphere. The role of PP and DD electric fields in affecting the ionosphere is clearly identified through the strengthening or weakening of EIA crests, enhancement or reduction of plasma densities and presence of EPBs. Table 1 summarizes the observations during different phases of the storm and their corresponding inferences. Figure 12 shows the solar wind parameters and geomagnetic indices (similar to Figure 1) narrowed down for the period of 23 April to midday of 26 April with durations of the PPEF and DDEF inferred in this work. The blue (red) shaded region represents the duration of PPEF (DDEF). We find that the response of low and midlatitudes are similar during this event except for the dawn sector of temporary recovery phase. During that period, a negative ionospheric storm was observed only over low latitudes below ∼20° dip latitudes.

During both the main phases, PPEF caused noticeable enhancements in the plasma densities in the dawn sector and stronger EIA in the dusk sector. Surprisingly, during the intermediate temporary recovery phase between first and second main phases, effect of PPEF was even stronger. Furthermore, even during the first 5 hours of the recovery phase, PPEF has dominated the ionosphere during this storm. This might have happened because of significant presence of eastward IEF E_Y though the

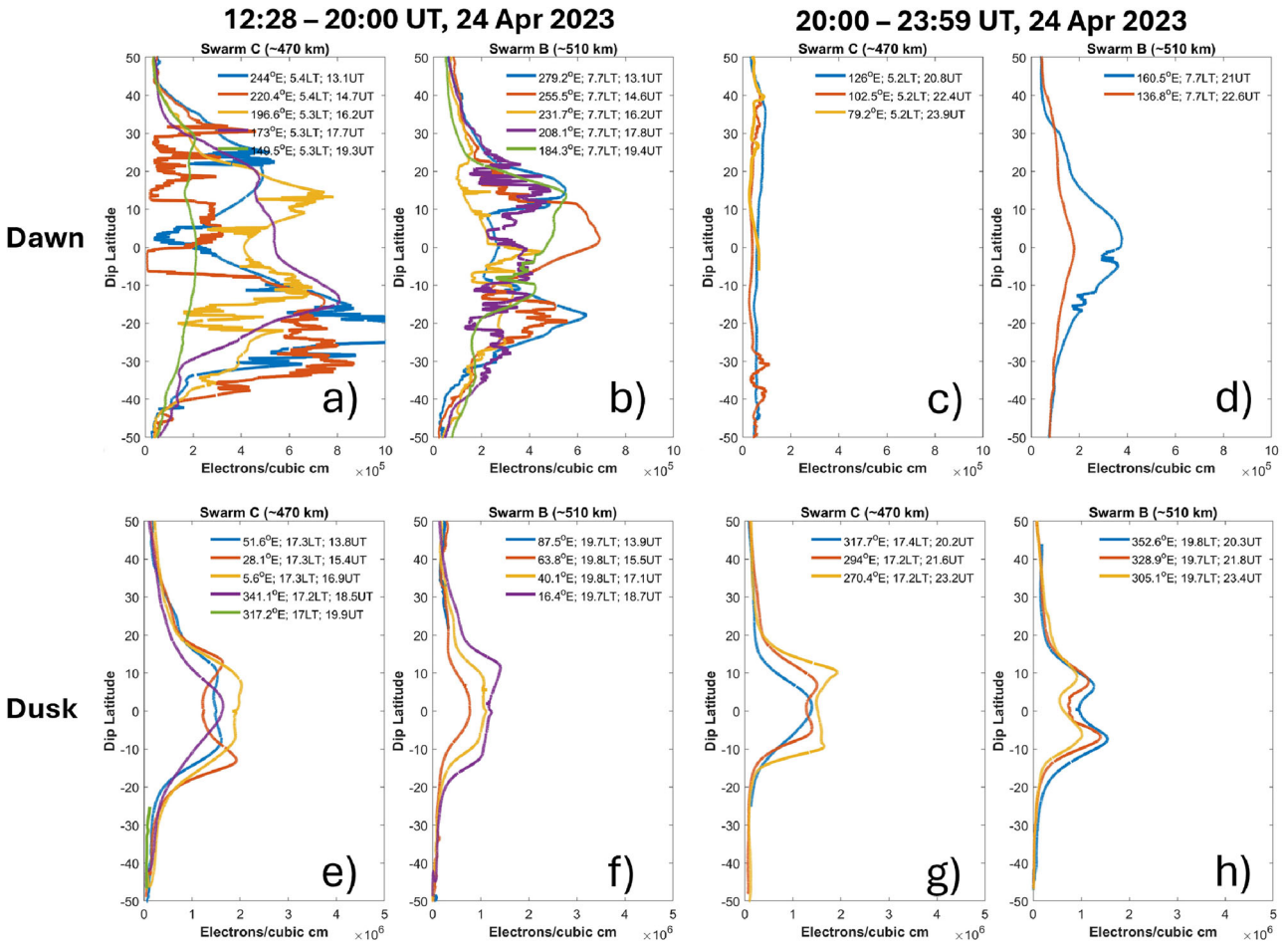

Figure 11. Observations during the late recovery phase of the storm on 24 April separated into two parts. First two columns show observations during 12:28 - 20:00 UT and the third and fourth columns show observations during 20:00 - 23:58 UT. The first row (**a-d**) shows dawn sector results and the second row (**e-h**) shows dusk sector results respectively.

recovery of ring current has commenced. Such observations show that to properly investigate ionospheric impacts, we need to consider both magnetic indices and solar wind parameters. Use of mere magnetic indices may not be enough to rightly predict the type of electric fields penetrating into the ionosphere. Thus, Swarm measurements indicate existence of a long lasting PPEF from the onset of the storm at 17:41 UT on 23 April to about 9:00 UT on 24 April, well into the early recovery phase (see Table 1, and the blue shaded region in Figure 12).

OS electric fields are expected at least for some duration in the temporary recovery phase or during the start of the early recovery phase. However, We did not succeed in identifying OS electric field effects in the ionosphere. Possible reasons might be either weak OS during this event or the OSEF was short lived so that the intermittent Swarm passes did not capture it in the latitudinal profiles. Disturbed thermospheric winds were inferred in this work through interpretation of the latitudinal plasma density gradients. DD electric field signatures are clearly identified between 9:00 - 20:00 UT on 24 April during the recovery phase of the storm (red shaded duration in Figure 12). However, DDEF were seen only after 4 hours into the recovery phase and has subsided well before the recovery of the ring current indicated by SYM-H index.

To conclude, the important inferences from this work are: (i) There was a long lasting PPEF for about 15 hours from the onset of the storm which extended even into the first 4-5 hours of the recovery phase. This was attributed to the fact that IMF B_Z and IEF E_Y are still strongly favorable for magnetospheric convection. (ii) No observations could be attributed to the OSEF even during periods when OSEF was supposed to occur. This indicates that probably shielding was weaker during this event enabling both a long lasting PPEF and lack of OSEF. (iii) DDEF effects were seen only after 4-5 hours

Table 1. Table summarizing observations during different phases of the storm and their interpretation

Storm phase	Dawn		Dusk	
	Swarm A and C	Swarm B	Swarm A and C	Swarm B
Main phases (23/04 17:41 - 21:26 UT and 24/04 01:36 - 04:03 UT	No clear effect	Clear plasma density enhance-ments - PPEF	No clear effect	Larger separation of EIA crests along with EPBs - PPEF
Temporary recovery phase 23/04 21:26 UT - 24/04 01:36 UT	Plasma density reduction in low latitudes (<20°dip latitudes) - PPEF	Clear plasma density enhance-ments in the equatorial and souther hemispheric regions - PPEF and altered winds	Stronger EIA - PPEF	Stronger EIA - PPEF
Early recovery phase before 09 UT on 24/04	No clear effect	Reversed plasma density gradient (Southward gradient) - Altered winds	Stronger EIA - PPEF	Stronger EIA - PPEF
Early recovery phase after 09 UT on 24/04	Strong EPBs and EIA in the presunrise period - DDEF	Clear plasma density enhancement over the southern hemisphere - probable role of altered winds	EIA inhibition - DDEF	EIA inhibition - DDEF
Late recovery phase before 20 UT on 24/04	Strong EPBs - DDEF	Strong EPBs - DDEF	EIA inhibition - DDEF	EIA inhibition - DDEF
Late recovery phase after 20 UT on 24/04	Ionosphere appeared to have recovered from storm effects			

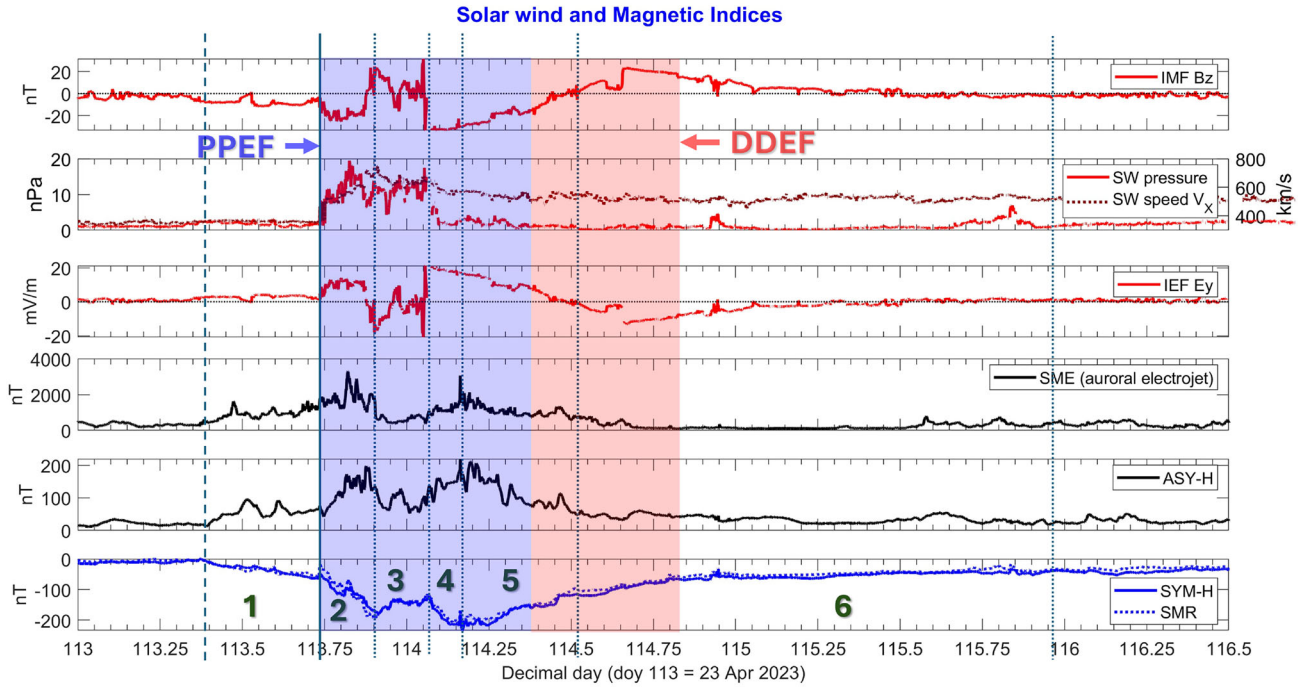

Figure 12. Solar wind parameters and geomagnetic indices as in Figure 1 are shown along with the duration of PPEF shaded in blue and DDEF shaded in red for the period of 00:00 UT on 23 April to 12:00 UT on 26 April 2023. It may be seen that long lasting PPEF is observed from the onset of the geomagnetic storm to early part of the recovery phase for about 15 hours, after which DDEF is observed for about 11 hours during the event.

into the recovery of the storm, and existed for 11 hours. And (iv) DDEF disappeared well before the recovery of the storm according to SYM-H (and SMR) indices. Therefore, we cannot predict the ionospheric response with mere magnetic indices and solar wind parameters. We need to measure the ionosphere to understand the response.

Acknowledgements

VLN acknowledges the support from Krea University research grant and Anusandhan National Research Foundation grant ANRF/ECRG/2024/002417/EAS. VLN also expresses sincere thanking to the ESA Swarm satellite team for providing Swarm satellite measurements used in this work (https://swarm-diss.eo.esa.int/). The author gratefully acknowledges the data of solar wind indices obtained from the NASA/GSFC Space Physics Data Facility (https://cdaweb.gsfc.nasa.gov/), magnetic indices from SuperMAG network (https://supermag.jhuapl.edu/indices/) and world data center, Kyoto (https://wdc.kugi.kyoto-u.ac.jp/index.html).

References

Abdu M. 2012, J. Atmos. Sol-Terr. Phys., 75–76, 44

Balan N., Bailey G. J. 1995, J. Geophys. Res. Space Physics, 100, 21421

Baruah Y., Roy S., Sinha S. *et al*. 2024, Space Weather, 22, e2023SW003716

Batista, I. S., Diogo, E. M., Souza, J. R., Abdu, M. A., & Bailey, G. J. 2011, Equatorial Ionization Anomaly: The Role of Thermospheric Winds and the Effects of the Geomagnetic Field Secular Variation, ed. M. A. Abdu & D. Pancheva (Dordrecht: Springer, Netherlands), 317–328.

Blanc M., Richmond A. 1980, J. Geophys. Res. Space Physics, 85, 1669

Borovsky J. E. 2021, Front. Astron. Space Sci., 8. https://doi.org/10.3389/fspas.2021.634073

Borovsky J. E., Denton M. H. 2006, J. Geophys. Res. Space Physics, 111, A07S08

Buonsanto M. 1999, Space Sci. Rev., 88, 563

Carter, B. A., Ram, S. T., Yizengaw, E., *et al.* 2018, Prog. Earth Planet Sci., 5, https://doi.org/10.1186/s40645-018-0164-y.

Currie J. L., Carter B. A., Retterer J. *et al*. 2021, J. Geophys. Res. Space Physics, 126, e2020JA028724

Fejer B. G., Scherliess L. 1997, J. Geophys. Res. Space Physics, 102, 24047

Fuller-Rowell T. J., Codrescu M. V., Moffett R. J., Quegan S. 1994, J. Geophys. Res. Space Physics, 99, 3893

Gjerloev J. W. 2012, J. Geophys. Res. Space Physics, 117, A09213
Gonzalez W. D., Joselyn J. A., Kamide Y. *et al*. 1994, J. Geophys. Res. Space Physics, 99, 5771
Hajra R., Tsurutani B. T., Lu Q. *et al*. 2024, J. Geophys. Res. Space Physics, 129, e2024JA032986
Hanson W. B., Moffett R. J. 1966, J. Geophys. Res., 71, 5559
Huang C. M. 2013, J. Geophys. Res. Space Physics, 118, 496
Huang C.-S. 2019, J. Geophys. Res. Space Physics, 124, 9640
Iyemori T. 1990, J. Geomag. Geoelect., 42, 1249
Jin H. 2009, Journal of the National Institute of Information and Communications Technology, 56, 209
Kepkar A., Arras C., Wickert J. *et al*. 2020, Ann. Geophys., 38, 611
Kikuchi, T. 2021, Penetration of the Magnetospheric Electric Fields to the Low Latitude Ionosphere (American Geophysical Union (AGU)), 313–338.
King J. 1968, J. Atmos. Terr. Phys., 30, 391
Laštovička J. 1996, J. Atmos. Terr. Phys., 58, 831
Li L., Jin S. 2024, J. Atmos. Sol-Terr. Phys., 259, 106238
Lyon J. G. 2000, Science, 288, 1987
Lyu H., Fang H., Meng X. 2022, Adv. Space Res., 70, 2081
Maruyama T., Matuura N. 1984, J. Geophys. Res., 89, 10903
Mošna Z., Barta V., Berényi K. A. *et al*. 2024, Front. Astron. Space Sci., 11,. https://doi.org/10.3389/fspas.2024.1462160
Narayanan V. L., Gurubaran S., Emperumal K., Patil P. 2013, J. Atmos. Sol-Terr. Phys., 103, 113
Narayanan V. L., Gurubaran S., Emperumal K., Patil P. T. 2011, J. Geophys. Res. Space Physics, 116, A09315
Narayanan V. L., Gurubaran S., Shiokawa K., Emperumal K. 2016, J. Geophys. Res. Space Physics, 121, 6924
Narayanan V. L., Sau S., Gurubaran S. *et al*. 2014, Earth Planet Space, 66, 160
Narayanan V. L., Wright C., Mlynczak M. *et al*. 2024, J. Geophys. Res. Space Physics, 129, e2023JA032157
Otsuka Y. 2018, Prog. Earth. Planet. Sci., 5, 57
Peymirat C., Richmond A. D., Kobea A. T. 2000, J. Geophys. Res. Space Physics, 105, 22991
PröLss, G. W. 2008, Ionospheric Storms at Mid-Latitude: A Short Review (American Geophysical Union (AGU)), 9–24.
Ranjan A. K., Sunil Krishna M. V., Kumar A. *et al*. 2023, J. Geophys. Res. Space Physics, 128, e2023JA032028
Rao S., Srivastava N., Chakrabarty D. 2025, J. Astrophys. Astron., 46, 37
Rishbeth, H., & Garriott, O. 1969, Introduction to Ionospheric Physics (Academic Press).
Rout D., Chakrabarty D., Sekar R. *et al*. 2016, J. Geophys. Res. Space Physics, 121, 4800
Spogli L., Alfonsi L., Cesaroni C. 2023, Space Weather, 21, e2022SW003331
Tsunoda R. T. 1985, J. Geophys. Res., 90, 447
Vasyliunas, V. M. 1970, in Particles and Fields in the Magnetosphere, ed. B. M. McCormac (Dordrecht: Springer, Netherlands), 60–71.
Vasyliunas, V. M. 1972, in Earth's Magnetospheric Processes, ed. B. M. McCormac (Dordrecht: Springer, Netherlands), 29–38.
Wolf R. A. 1970, J. Geophys. Res., 75, 4677